

Article

Effect of Lime on Stability of Chromium in Stainless Steel Slag

Qing Zhao ^{1,2,*}, Chengjun Liu ^{1,2}, Longhu Cao ³, Xiang Zheng ^{1,2} and Maofa Jiang ^{1,2}

¹ Key Laboratory for Ecological Metallurgy of Multimetallic Minerals (Ministry of Education), Northeastern University, Shenyang 110819, China; liucj@smm.neu.edu.cn (C.L.); xiangzheng222A@gmail.com (X.Z.); jiangmf@smm.neu.edu.cn (M.J.)

² School of Metallurgy, Northeastern University, Shenyang 110819, China

³ WISDRI Engineering & Research Incorporation Limited, Wuhan 430223, China; 03110@wisdri.com

* Correspondence: zhaohq@smm.neu.edu.cn; Tel.: +86-151-4004-8687 or +86-024-8368-1478

Received: 17 August 2018; Accepted: 25 September 2018; Published: 26 September 2018



Abstract: The stabilization of chromium is of great importance to the use of stainless steel slag (SSS), and the influence of lime on the stability of chromium is currently unclear. In this work, the variation of phase transformation and chromium distribution with slag basicity (CaO/SiO₂) were investigated experimentally, and the leaching ability of chromium was evaluated. Results showed that chromium-bearing phases were glass, dicalcium silicate (C₂S), spinel, and periclase, while the degree of enrichment of chromium in these phases was found to be closely related to the basicity. The optimal basicity obtained in this research was 1.5, with the chromium mainly present in the stable spinel and exhibiting the lowest leaching ability. The product layer structure of unmelted lime was studied as well, showing a periclase layer and a Ca₂SiO₄ layer. Some CaCr₂O₄ had formed in the periclase layer, which is potentially hazardous for the environment and living organisms.

Keywords: stainless steel slag; lime; basicity; phase transformation; chromium pollution

1. Introduction

A large amount of chromium-bearing stainless steel slag (SSS) is generated during stainless steel production, and discharging this into the environment gives severe pollution issues [1]. Some chromium exists in unstable phases, like dicalcium silicate (Ca₂SiO₄, nominated as C₂S in this study), merwinite (Ca₃MgSi₂O₈), melilite (Ca₂Mg₂SiO₇), gehlenite (Ca₂Al₂SiO₇), and periclase (MgO). Cr²⁺ and Cr³⁺ can be released after phase decomposition, followed by oxidation to hexavalent chromium (Cr⁶⁺). The latter is known to be a carcinogen, and a dermatological and pulmonary sensitizer that is 500 times more toxic than Cr³⁺ [2–4]. In order to reduce the harmful effects of chromium, a lot of effort has been focused on controlling chromium distribution across the various phases. Our previous work has shown that chromium-bearing spinel does not notably corrode, even in an extremely acidic solution (80 wt % sulfuric acid, 160 °C) [5]. Therefore, the method of enriching the chromium into a stable spinel phase is attracting extensive attention [6–8], and a molten modification using spinel forming agents was reported to improve spinel growth and restrict chromium leaching [9].

For the purposes of dephosphorization and desulfurization, a certain amount of lime must be added to the molten slag [10]. The basicity of slag (the mass ratio of basic components to acidic components) increases with lime fusing, which causes a variation of elemental distributions in various phases [11–13]. However, there are discrepancies in the literature regarding the influence of the basicity of slag on the chromium migration behavior in the SSS. Mostafaei and Jönsson found that the basicity had almost no effect on the amount of spinel phase in slag [14], while some other researchers hold different opinions. Engström et al. reported basicity to have a strong impact on the chromium

distribution in the SSS [15], and Albertsson et al. pointed out that a high basicity (>1.4 in their study) should be avoided, since it can lead to the formation of leachable chromium-bearing solid solutions [16]. The optimal value of basicity for enriching chromium in the spinel phase, as obtained from various research works, is closely related to the slag composition the researchers used [17,18]. Wang and Seetharaman investigated the oxidation state of chromium oxides in $\text{CaO-SiO}_2\text{-CrO}_x$ and $\text{CaO-MgO-(FeO-)}\text{Al}_2\text{O}_3\text{-SiO}_2\text{-CrO}_x$ using X-ray absorption near edge structure (XANES) analysis, and found that the mass ratio $X_{\text{CrO}}/X_{\text{CrO}_{1.5}}$ increased with decreasing slag basicity, while, beyond a certain level, the ratio was unaffected by basicity [19].

Another noteworthy issue is that the lime readily reacts with SiO_2 , forming a C_2S product layer at the interface, which could prevent the lime from dissolving into the molten slag [20,21]. The unmelted lime in the SSS would expand and blast when it contacts water [22,23]. As a consequence, some chromium-bearing powders erupt from the slag and after transfer by air, endangering a larger area. However, the details of the structure around the unmelted lime are poorly understood, and the possible pollution caused by this is, therefore, difficult to quantify.

In this paper, in order to clarify the effect of lime (melted, melting, or solid) on the stability of chromium in SSS, the variation of phase transformation and chromium distribution with basicity as well as the leaching ability of chromium were experimentally investigated. Moreover, the microstructure of the product layer around the unmelted lime was studied.

2. Materials and Methods

2.1. Materials

Based on a typical composition of SSS from a stainless steel plant, experimental slags with different basicities (the mass ratio of CaO to SiO_2 , B) of 1.0 (S1), 1.5 (S2), and 2.0 (S3) were prepared by chemical reagents calcium oxide ($\text{CaO} \geq 98.0$ wt %), silicon oxide ($\text{SiO}_2 \geq 99.0$ wt %), magnesium oxide ($\text{MgO} \geq 99.9$ wt %), aluminum oxide ($\text{Al}_2\text{O}_3 \geq 99.0$ wt %), ferrous oxalate ($\text{FeC}_2\text{O}_4 \cdot 2\text{H}_2\text{O} \geq 99.9$ wt %), chromium oxide ($\text{Cr}_2\text{O}_3 \geq 99.0$ wt %), and calcium fluoride ($\text{CaF}_2 \geq 98.5$ wt %), respectively. All reagents were purchased from Sinopharm Chemical Reagent Co., Ltd., Shenyang, China, and were dried at 110 °C for 10 h before weighing and mixing. One sample (S4) without Cr_2O_3 was also prepared for a control experiment with unmelted lime. The chemical compositions of the target SSS samples (S1–S4) are shown in Table 1. Some CaO lumps ($6 \text{ mm} \times 6 \text{ mm} \times 8 \text{ mm}$) were prepared from CaO powder by briquetting and polishing treatments and used as unmelted lime.

Table 1. Chemical composition of the target stainless steel slag, wt % and index of basicity, B .

No.	CaO	SiO ₂	MgO	Al ₂ O ₃	FeO	Cr ₂ O ₃	CaF ₂	B
S1	38.0	38.0	9.0	4.0	3.0	5.0	3.0	1.0
S2	45.6	30.4	9.0	4.0	3.0	5.0	3.0	1.5
S3	50.6	25.4	9.0	4.0	3.0	5.0	3.0	2.0
S4	48.6	32.4	9.0	4.0	3.0	0	3.0	1.5

2.2. Methods

The experimental furnace employed in this study is equipped with a MoSi_2 heater and is controlled by a PID controller equipped with a PtRh30%/PtRh6% thermocouple sensor, which is illustrated in Figure 1. The temperature deviation at the constant temperature zone is less than ± 2 °C.

Slag (10 g) was poured into a molybdenum crucible inside a graphite crucible. The molybdenum crucible is used to protect the graphite crucible and for easy sampling. The graphite crucible was placed in the constant-temperature zone of the furnace. High purity argon was injected from the bottom of the furnace at a flow rate of $0.5 \text{ L} \cdot \text{min}^{-1}$ to protect the samples from oxidation. The slags were heated to 1600 °C at a rate of 3 °C $\cdot\text{min}^{-1}$, and held for 30 min at 1600 °C to achieve a fully molten state,

after which the molybdenum crucible was taken out of the furnace followed by cooling. Two different cooling treatment routes were adopted: (1) direct quenching in water at 1600 °C after incubation for 30 min; (2) incubation for 30 min, cooled to 1300 °C at a cooling rate of 3 °C/min and then incubation for 30 min before quenching with water. Theoretical calculations using FactSage (developed jointly between Thermfact/CRCT and GTT-Technologies, Version 7.0, Montreal, Canada and Aachen, Germany) and pilot experiments both showed that the phase transformation and chromium migration hardly change below 1300 °C.

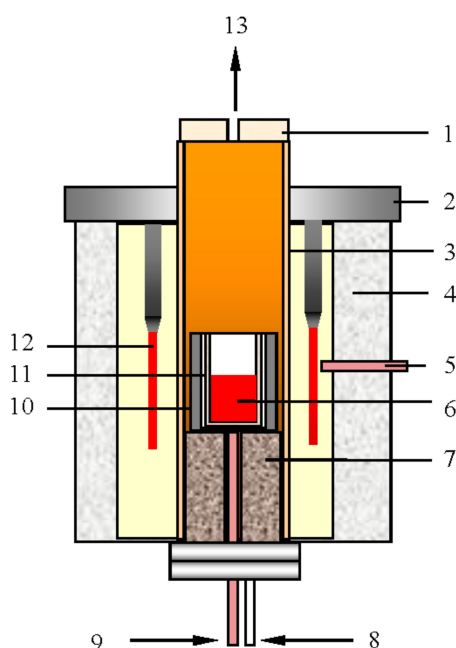


Figure 1. Illustration of the experimental furnace used in this study. 1—cap; 2—furnace cover; 3—corundum tube; 4—insulation layer; 5—thermocouple A; 6—stainless steel slag; 7—refractory; 8—gas inlet; 9—thermocouple B; 10—graphite crucible; 11—molybdenum crucible; 12—MoSi₂ heating elements; 13—gas outlet.

Moreover, 30 g of samples S2 and S4 were used for the unmelted lime study. When the slag completely molten, the as-prepared CaO lump was immersed into the melt and held in place for 20 min at 1600 °C, after which the crucible was taken out of the furnace and cooled under the air atmosphere. Polishing and gold spraying processes were conducted on the samples, to give them conductivity for scanning electric microscope-energy dispersive spectroscopy (SEM-EDS) analysis.

SEM-EDS analysis was conducted using the Hitachi S3400N scanning electron microscope (HITACHI, Tokyo, Japan) equipped with an INCA 3294 EDS system (HITACHI, Tokyo, Japan) to investigate the microstructure and chemical composition of the precipitated phases. The law of conservation of mass and linear least sum of squares methods were adopted to calculate the composition of the precipitated phase, and the distribution of chromium across the various phases was evaluated by calculating an enrichment degree of chromium ($E_{Cr,i}$). The $E_{Cr,i}$ is defined as

$$E_{Cr,i} = \frac{(\%Cr)_i X_i^*}{\sum_{i=1}^n (\%Cr)_i X_i^*} \times 100\%, \quad (1)$$

where i is a specific phase; $(\%Cr)_i$ is the chromium content in a specific phase, wt %; and X_i^* is the normalized mass fraction of a specific phase.

The phase composition of each sample was analyzed using Philips X'pert X-ray diffraction (XRD) with a Cu K α source ($\lambda = 1.5418 \text{ \AA}$) over the range $2\theta = 10\text{--}80^\circ$, at a step of 0.008° , and specified by

to have a positive effect on the activity coefficient of the MgO and CrOx, which leads to a decrease of spinel solubility in the liquid [24,25]. This is presumably the reason for the precipitation of spinel in S2 at 1600 °C. Furthermore, the C₂S disappeared, and a new phase of chromium-free merwinite precipitated when the temperature decreased to 1300 °C. This suggests that the growth of spinel crystal during the cooling process requires a Cr₂O₃ feed, which causes a driving force for chromium transport from other phases to the spinel. Moreover, the solid solubility of Cr₂O₃ in the precipitated silicate phases decreases with temperature, and eliminated Cr₂O₃ from the silicate phases.

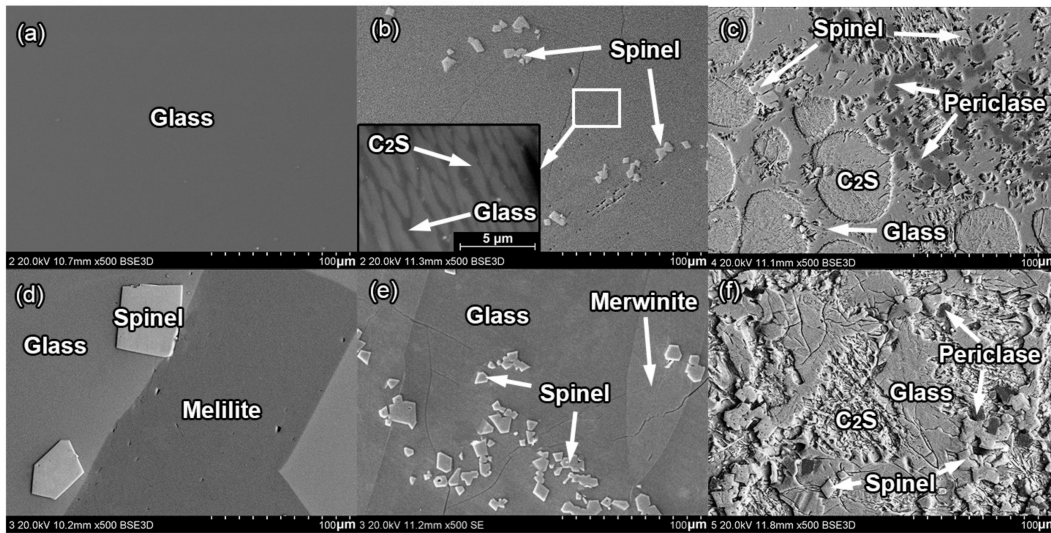


Figure 3. SEM-EDS results of S1, S2, and S3 quenched at 1600 and 1300 °C. (a) $B = 1.0$, 1600 °C; (b) $B = 1.5$, 1600 °C; (c) $B = 2.0$, 1600 °C; (d) $B = 1.0$, 1300 °C; (e) $B = 1.5$, 1300 °C; (f) $B = 2.0$, 1300 °C.

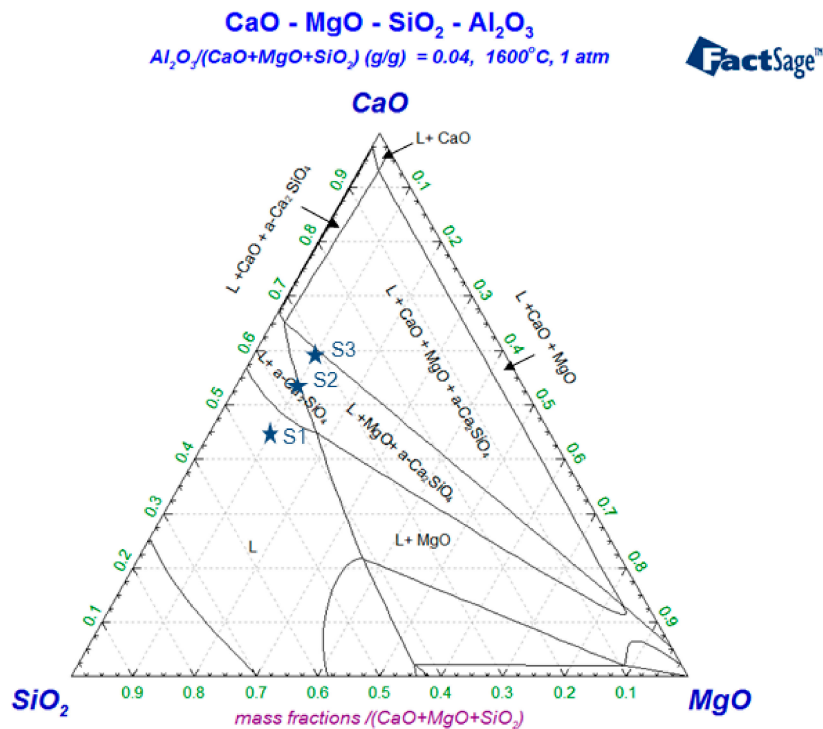


Figure 4. Isothermal section diagram of the CaO–SiO₂–MgO–4%Al₂O₃ slag system.

As shown in Figures 2c and 3c,f, besides the phases of the spinel, glass, and C₂S, a periclase phase formed in sample S3 ($B = 2.0$). Figure 4 shows the composition of S3 to be located in the phase equilibrium zone of liquid + MgO + C₂S. Therefore, the precipitation of periclase is explained

by thermodynamics when the basicity is 2.0. Furthermore, chromium was only detected in the spinel and with periclase, while other phases of glass and C_2S were determined to be chromium-free. The explanation for this phenomenon can be found in the binary phase diagram of $MgO-Cr_2O_3$, showing that Cr_2O_3 can dissolve into MgO at high temperature [26]. No change in phase composition of S3 was observed after the cooling process from 1600 to 1300 °C.

3.2. Distribution and Stability of Chromium

The enrichment degree of chromium in each phase of the various samples was calculated and illustrated in the form of pie charts, as shown in Figure 5. Furthermore, a batch of standard leaching tests was conducted for these samples to evaluate the leaching ability of chromium, and the corresponding results are also provided in Figure 5.

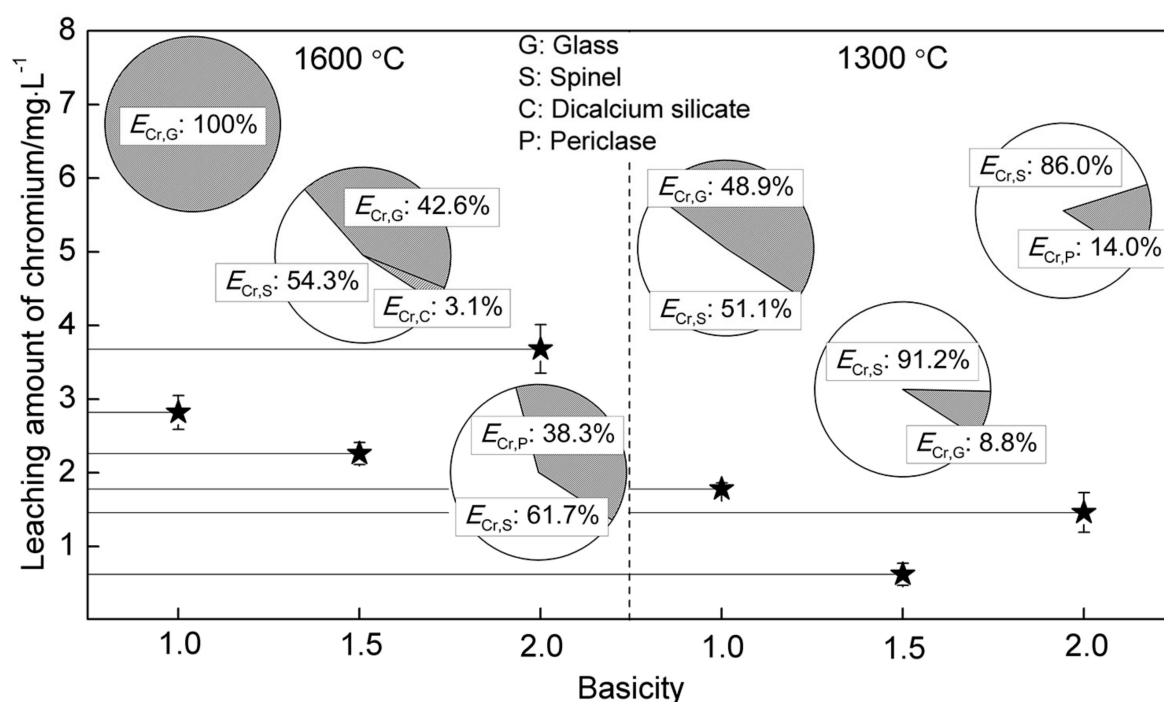


Figure 5. Distribution (pie chart) and leaching amount of chromium of S1, S2, and S3 quenched at 1600 and 1300 °C.

Results indicated that, at 1600 °C (cf. the left-hand side of Figure 5), when $B = 1.0$, all of the chromium existed in the glass phase, and when the basicity increased to 1.5, about 54.3% and 3.1% of chromium were in the spinel phase and C_2S , respectively. The migration of chromium from glass to spinel phase caused a decrease in the leached amount of chromium, from 2.82 to 2.26 $mg \cdot L^{-1}$. When $B = 2.0$, about 61.7% of the chromium existed in the spinel phase and the remainder dissolved in the periclase phase. The leached amount of chromium reached 3.68 $mg \cdot L^{-1}$ as a result of the low stability of the periclase phase in acid solution. When the samples were cooled to 1300 °C (cf. the right hand side of the Figure 5), more chromium migrated into the spinel phase: the $E_{Cr,S}$ of S1, S2, and S3 were 51.1%, 91.2%, and 86.0%, respectively. Moreover, the lowest leached amount of chromium was 0.62 $mg \cdot L^{-1}$, obtained when the basicity was 1.5. On the basis of the findings of this work, it can be proposed that the CaO content in SSS has a significant effect on the distribution and stability of chromium, and the optimal basicity was 1.5 from the viewpoint of chromium retention.

3.3. Product Layer Structure of Unmelted Lime

To study the effects of unmelted lime on the stability of chromium in SSS, CaO lumps were immersed into the molten samples S2 (5% Cr_2O_3 , $B = 1.5$) and S4 (Cr_2O_3 free, $B = 1.5$), and held in

place for 20 min at 1600 °C. XRD analysis was then carried out for investigating the phase composition of the S2 and S4 treated by the CaO lump, giving the results shown in Figure 6. The C_2S , merwinite, spinel, periclase phases were identified in both samples, and the diffraction peaks of $CaCr_2O_4$ was detected in the XRD pattern of Cr_2O_3 -bearing S2.

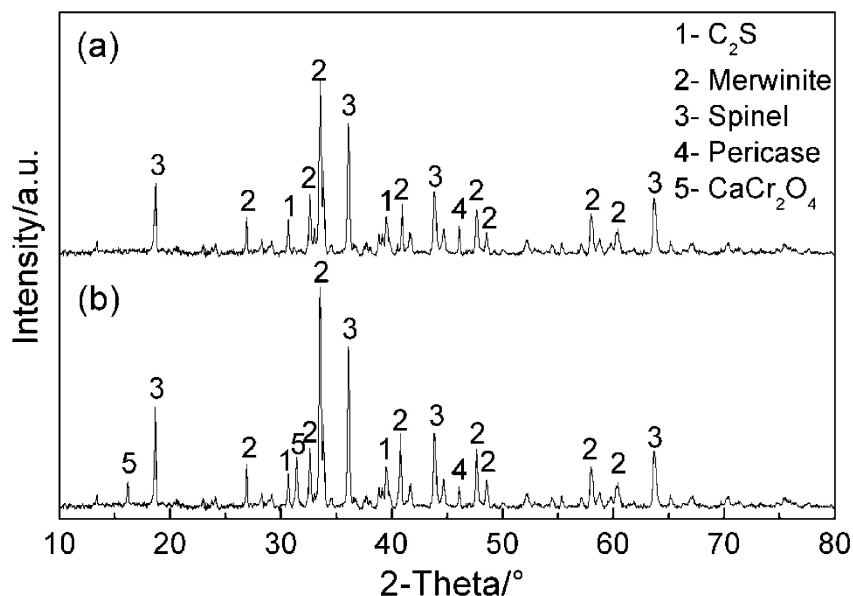


Figure 6. XRD patterns of (a) S4 and (b) S2 treated by a CaO lump.

Figure 7 shows the SEM images of the interface zone between the CaO lump and the slag. As shown in Figure 7a, four phases can be identified in for sample S4. The phase at lower left-hand corner is the unmelted CaO lump, while the top right-hand corner shows the slag containing precipitated spinel, merwinite, and C_2S phase. A 10–30 micron thick product layer was formed between the two phases, which consisted of a periclase layer (next to the CaO lump) and a C_2S layer (next to the slag). Based on the analysis of the Figure 4, it can be inferred that some CaO gradually dissolved into the molten slag with time, causing an increase in basicity around the CaO lump, which resulted in the precipitation of MgO and C_2S at the interface zone between the CaO lump and slag.

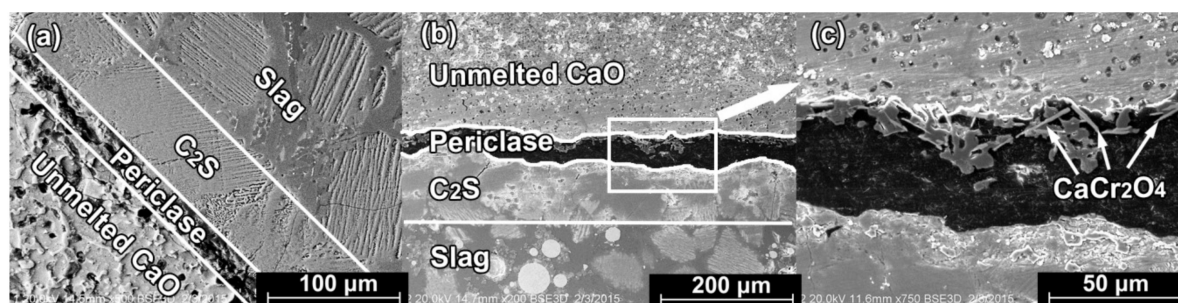


Figure 7. SEM images of interface zone between (a) CaO lump and S4; (b) and (c) CaO lump and S2.

Besides the findings previously obtained, a clear crack in the periclase layer was observed in S2 (cf. Figure 7b,c). A needle-shaped phase was detected at the fracture surface which, using EDS analysis, was determined to be the $CaCr_2O_4$ [27]. The binary phase diagram of Ca– Cr_2O_3 is provided in Figure 8a, giving evidence for the possibility of $CaCr_2O_4$ precipitation around the CaO lump. An Eh–pH diagram of Ca–Cr– H_2O at 25 °C was calculated using FactSage 7.0, and given in Figure 8b, showing that $CaCr_2O_4$ is unstable in an acid solution and an oxidizing environment. The Cr^{3+} can

be released from the slag and dispersed by water, and a toxic chromium chromate could be formed that causes serious pollution issues. Moreover, it was found that the periclase phase contained some chromium, while the C_2S was chromium-free. The sample S2 treated with a CaO lump was crushed and milled into powder, and a leaching test was conducted to determine the chromium stability. Results indicated that the chromium concentration in the leachate was about $3.73 \text{ mg}\cdot\text{L}^{-1}$ chromium, which is much higher than that of the untreated S2 (cf. Figure 5).

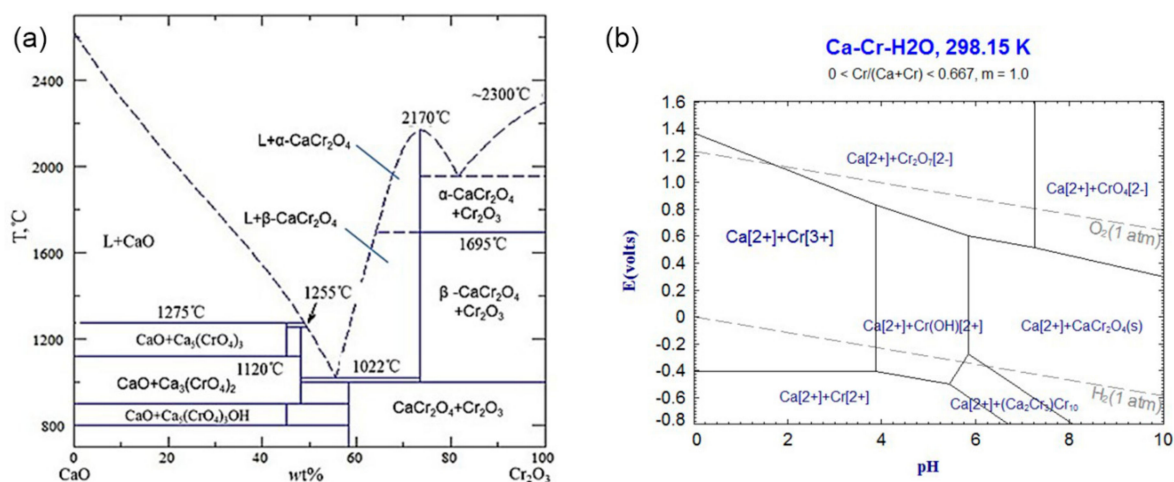


Figure 8. (a) Binary phase diagram of CaO–Cr₂O₃ and (b) Eh–pH diagram of Ca–Cr–H₂O systems at 25 °C.

It is noteworthy that the unmelted lime could react with water and produce Ca(OH)₂, which can result in volume expansion and pulverization of slag, which aggravates the possible chromium pollution. As stated above, the unmelted lime has an adverse impact on the security of SSS application.

4. Conclusions

The effect of lime on the stability of chromium in stainless steel slag (SSS) was investigated in this work. Experimental results showed that glass, dicalcium silicate (C₂S), spinel, and periclase are the chromium-bearing phases present in SSS, and that the enrichment degree of chromium in these phases is closely related to the basicity. The optimal basicity was found to be 1.5, at which the chromium mainly existed in the stable spinel phase, and exhibited the lowest leaching amount: 2.26 and 0.62 mg·L⁻¹ for 1600 and 1300 °C, respectively. Moreover, the details of the product layer structure of unmelted lime were studied. It was found that the product layer consisted of a periclase layer (next to the CaO lump) and a C₂S layer (next to the slag), while some CaCr₂O₄ was detected in the periclase layer, which poses a threat to the environment and living organisms. Therefore, the amount and particle size of lime for slagging need to be controlled in view of the chromium retention.

Author Contributions: Experiment, Q.Z., L.C. and X.Z.; Data Analysis and Writing—Original Draft Preparation, Q.Z. and C.L.; Writing—Review & Editing, C.L. and M.J.

Funding: This research was supported the National Natural Science Foundation of China (No. 51704068), the National Key R&D Program of China (No. 2017YFC0805100) and the Fundamental Research Funds for the Central Universities (No. N172504020).

Acknowledgments: The authors gratefully acknowledge support from the National Natural Science Foundation of China (No. 51704068), the National Key R&D Program of China (No. 2017YFC0805100), the Fundamental Research Funds for the Central Universities (No. N172504020). Ron Zevenhoven of Åbo Akademi University, Turku, Finland, is acknowledged for checking and commenting on the manuscript.

Conflicts of Interest: The authors declare no conflict of interest.

References

1. Pillay, K.; Von, B.H.; Petersen, J. Ageing of chromium(III)-bearing slag and its relation to the atmospheric oxidation of solid chromium(III)-oxide in the presence of calcium oxide. *Chemosphere* **2003**, *52*, 1771–1779. [[CrossRef](#)]
2. Rai, D.; Sass, B.M.; Moore, D.A. Chromium-(III) hydrolysis constants and solubility of chromium(III) hydroxide. *Inorg. Chem.* **1987**, *26*, 345–349. [[CrossRef](#)]
3. Samada, Y.; Miki, T.; Hino, M. Prevention of chromium elution from stainless steel slag into seawater. *ISIJ Int.* **2011**, *51*, 728–732. [[CrossRef](#)]
4. Kan, C.C.; Ibe, A.H.; Rivera, K.K.P.; Arazo, R.O.; Luna, M.D.G.D. Hexavalent chromium removal from aqueous solution by adsorbents synthesized from groundwater treatment residuals. *Sustain. Environ. Res.* **2017**, *27*, 163–171. [[CrossRef](#)]
5. Zhao, Q.; Liu, C.J.; Li, B.K.; Jiang, M.F. Decomposition mechanism of chromite in sulfuric acid-dichromic acid solution. *Int. J. Min. Met. Mater.* **2017**, *24*, 1361–1369. [[CrossRef](#)]
6. Real, H.C.; Serrano, A.; Zeifert, B.H.; Ramirez, A.H.; Lopez, M.H.; Ramirez, A. Effect of MgO and CaO/SiO₂ on the immobilization of chromium in synthetic slags. *J. Mater. Cycles Waste* **2012**, *14*, 317–324. [[CrossRef](#)]
7. Torres, V.A.; Romero, A.; Zeifert, B.H.; Rivera, J.C.; Sánchez, P.F.; Cruz, A. Stabilization of MgCr₂O₄ spinel in slags of the SiO₂-CaO-MgO-Cr₂O₃ system. *Rev. Metal. Madr.* **2006**, *42*, 417–424. [[CrossRef](#)]
8. Drissen, P.; Andreas, E.; Michael, K.; Dirk, M. Recent development in slag treatment and dust recycling. *Steel Res. Int.* **2009**, *80*, 737–745. [[CrossRef](#)]
9. García-Ramos, E.; Romero-Serrano, A.; Zeifert, B.; Flores-Sánchez, P.; Hallen-López, M.; Palacios, E.G. Immobilization of chromium in slags using MgO and Al₂O₃. *Steel Res. Int.* **2008**, *79*, 332–339. [[CrossRef](#)]
10. Suito, H.; Inoue, R. Behavior of phosphorous transfer from CaO-Fe_tO-P₂O₅-(SiO₂) slag to CaO particles. *ISIJ Int.* **2006**, *46*, 180–187. [[CrossRef](#)]
11. Johnston, M.D.; Barati, M. Effect of slag basicity and oxygen potential on the distribution of boron and phosphorus between slag and silicon. *J. Non-Cryst. Solids* **2011**, *357*, 970–975. [[CrossRef](#)]
12. Johnston, M.D.; Jahanshahi, S.; Zhang, L.; Lincoln, F.J. Effect of slag basicity on phase equilibria and selenium and tellurium distribution in magnesia-saturated calcium iron silicate slags. *Metall. Mater. Trans. B* **2010**, *41*, 625–635. [[CrossRef](#)]
13. Jiang, T.; Wang, S.; Guo, Y.F.; Chen, F.; Zheng, F.Q. Effects of basicity and MgO in slag on the behaviors of smelting vanadium titanomagnetite in the direct reduction-electric furnace process. *Metals* **2016**, *6*, 107. [[CrossRef](#)]
14. Mostafae, S.; Jönsson, P. Influence of slag properties on the amount of solid precipitates in high-chromium EAF steelmaking. *Steel Grips J. Steel Relat. Mater.* **2011**, *9*, 355–359.
15. Engström, F.; Adolfsson, D.; Yang, Q.; Samuelsson, C.; Björkman, B. Crystallization behaviour of some steelmaking slags. *Steel Res. Int.* **2010**, *81*, 362–371. [[CrossRef](#)]
16. Albertsson, G.J.; Teng, L.; Björkman, B. Effect of basicity on chromium partition in CaO-MgO-SiO₂-Cr₂O₃ synthetic slag at 1873 K. *Miner. Process. Extr. Metall. Rev.* **2014**, *123*, 116–122. [[CrossRef](#)]
17. Morita, K.; Tsukiashi, K.; Kimura, M.; Sano, N. Activity of chromium oxide in CaO-SiO₂ based slags at 1873 K. *Steel Res. Int.* **2005**, *76*, 279–283. [[CrossRef](#)]
18. Wu, X.R.; Dong, X.M.; Wang, R.T.; Lv, H.H.; Cao, F.B.; Shen, X.M. Crystallization behaviour of chromium in stainless steel slag: Effect of FeO and basicity. *J. Residuals Sci. Technol.* **2016**, *13*, S57–S62. [[CrossRef](#)]
19. Wang, L.J.; Seetharaman, S. Experimental studies on the oxidation states of chromium oxides in slag systems. *Metall. Mater. Trans. B* **2010**, *41*, 946–954. [[CrossRef](#)]
20. Yang, X.; Matsuura, H.; Tsukihashi, S. Condensation of P₂O₅ at the interface between 2CaO-SiO₂ and CaO-SiO₂-FeO_x-P₂O₅ slag. *ISIJ Int.* **2009**, *49*, 1298–1307. [[CrossRef](#)]
21. Hamano, T.; Fukagai, S.; Tsukihashi, F. Reaction mechanism between Solid CaO and FeO_x-CaO-SiO₂-P₂O₅ slag at 1573 K. *ISIJ Int.* **2006**, *46*, 490–495. [[CrossRef](#)]
22. Deng, T.; Gran, J.; Du, S.C. Dissolution of lime in synthetic 'FeO'-SiO₂ and CaO-'FeO'-SiO₂ slags. *Steel Res. Int.* **2010**, *81*, 347–355. [[CrossRef](#)]
23. Li, Z.; Whitwood, M.; Millman, S.; Boggelen, J. Dissolution of lime in BOS slag: From laboratory experiment to industrial converter. *Ironmak. Steelmak.* **2014**, *41*, 112–120. [[CrossRef](#)]

24. Pretorius, E.B.; Muan, A. Oxidation state of chromium in CaO-Al₂O₃-CrO_x-SiO₂ melts under strongly reducing conditions at 1500 °C. *J. Am. Ceram. Soc.* **1992**, *75*, 1364–1377. [[CrossRef](#)]
25. Pretorius, E.B.; Muan, A. Activity-composition relations of chromium oxide in silicate melts at 1500 °C under strongly reducing conditions. *J. Am. Ceram. Soc.* **1992**, *75*, 1364–1377. [[CrossRef](#)]
26. Alper, A.M.; McNally, R.N.; Doman, R.C.; Keihn, F.G. Phase equilibria in the system MgO-MgCr₂O₄. *J. Am. Ceram. Soc.* **1964**, *47*, 30–33. [[CrossRef](#)]
27. Burja, J.; Tehovnik, F.; Medved, J.; Godec, M.; Knap, M. Chromite spinel formation in steelmaking slags. *Mater. Tehmol.* **2014**, *48*, 753–756.



© 2018 by the authors. Licensee MDPI, Basel, Switzerland. This article is an open access article distributed under the terms and conditions of the Creative Commons Attribution (CC BY) license (<http://creativecommons.org/licenses/by/4.0/>).